Supporting Information

for

Copper Vananate Nanobelts as Anodes for Photoelectrochemical Water Splitting: Influence of CoOx Overlayers on Functional Performances

Leonardo Girardi, [†] *Gian Andrea Rizzi,**[,†] *Lorenzo Bigiani,*[†] *Davide Barreca,*[‡] *Chiara Maccato*[†], *Carla Marega*[†] *and Gaetano Granozzi*[†]

[†] Department of Chemical Sciences, Padova University and INSTM, 35131 Padova, Italy

[‡] CNR-ICMATE and INSTM, Department of Chemical Sciences, Padova University, 35131 Padova, Italy

* Author to whom correspondence should be addressed; E-mail: gianandrea.rizzi@unipd.it

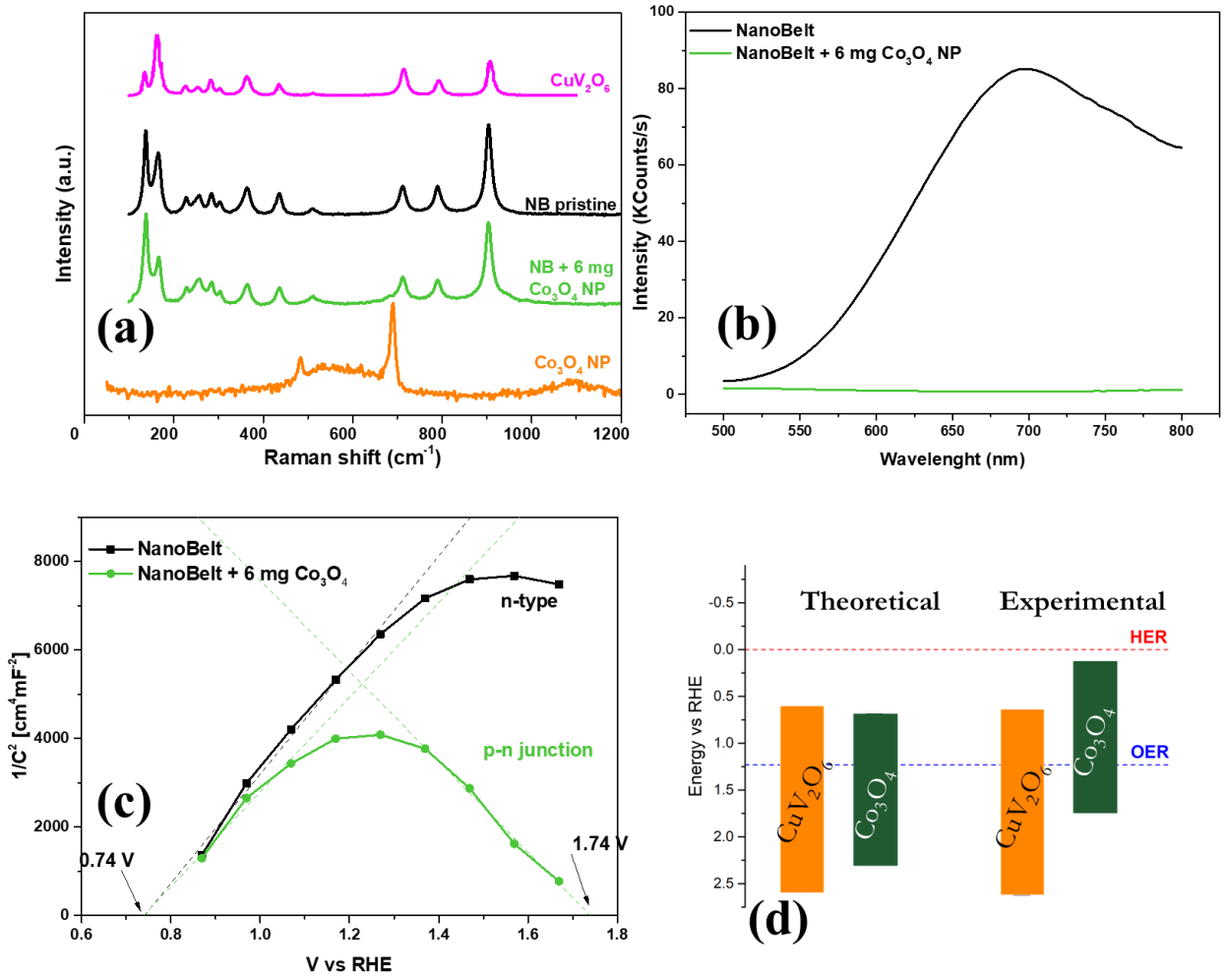

Figure S1. Preliminar data taken on a sample of CuV_2O_6 Nanobelt(NB), with 6 mg of Co_3O_4 nanoparticles (NP) deposited by drop-casting. The presence of the NP on the sample was confiremd by Raman spectra (a); the shoulder at around 700 cm^{-1} can be related to the presence of the NP(a). The sample was tested also for the pholuminesence, and the addition of the nanoparticles significantly reduced the charge recombination with radiative processes (b). The Mott-Schottky plot (c) evidences the successful formation of a *p-n* junction and the favorable band alignment (d).

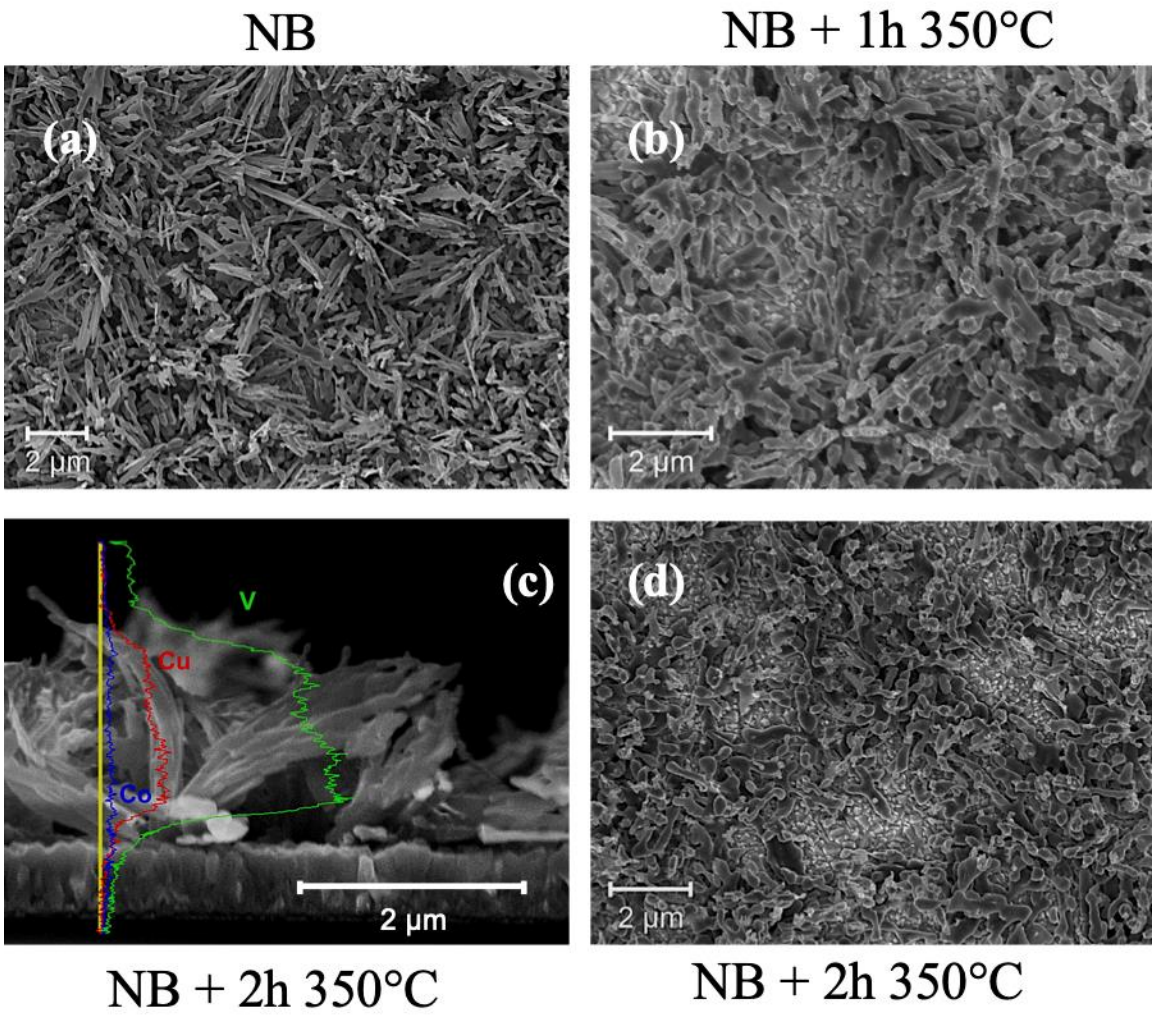

Figure S2. FE-SEM images for: (a) the NB specimen after annealing in air at 450°C for 1 h; (b,d) the NB 1h and NB 2h samples; (c) cross-sectional EDXS analysis of the NB 2h sample. Color codes: V, (green; Cu, red; Co, blue).

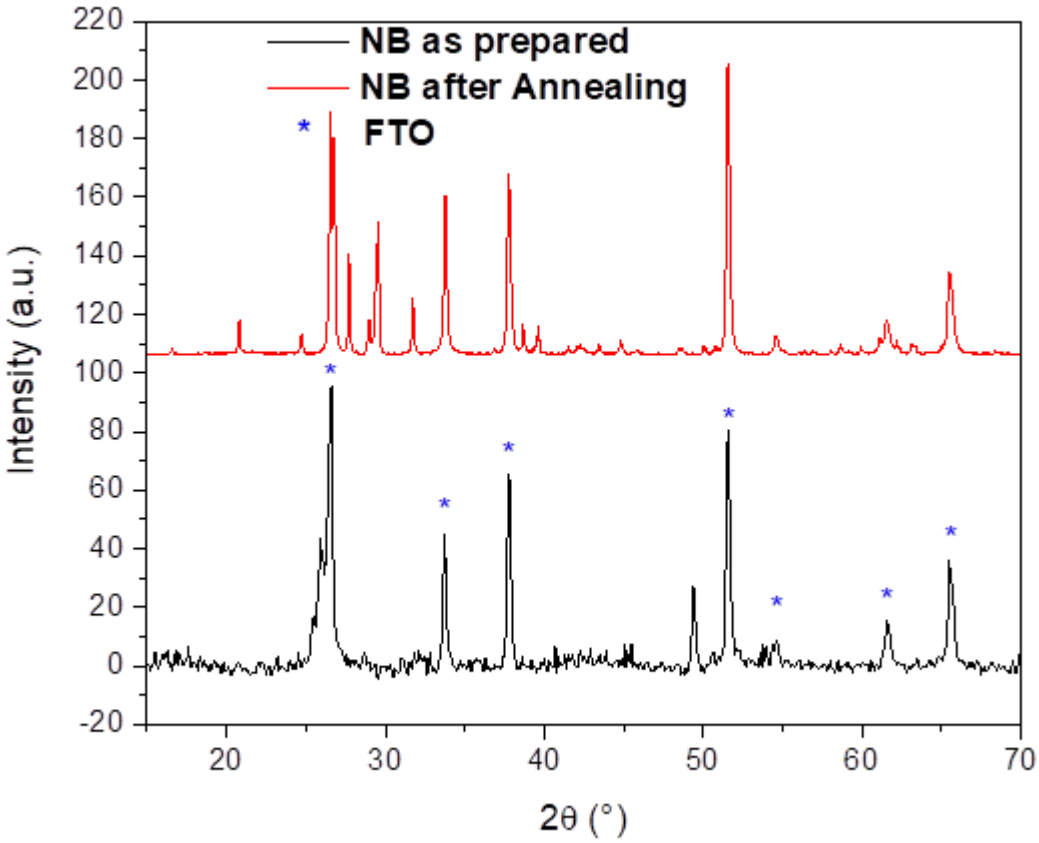

Figure S3. X-ray Diffraction (XRD) spectra of the target specimens before and after thermal treatment in air at 450°C for 1 h. The peaks from the substrate (Fluorine Tin Oxide FTO) are labelled with (*).

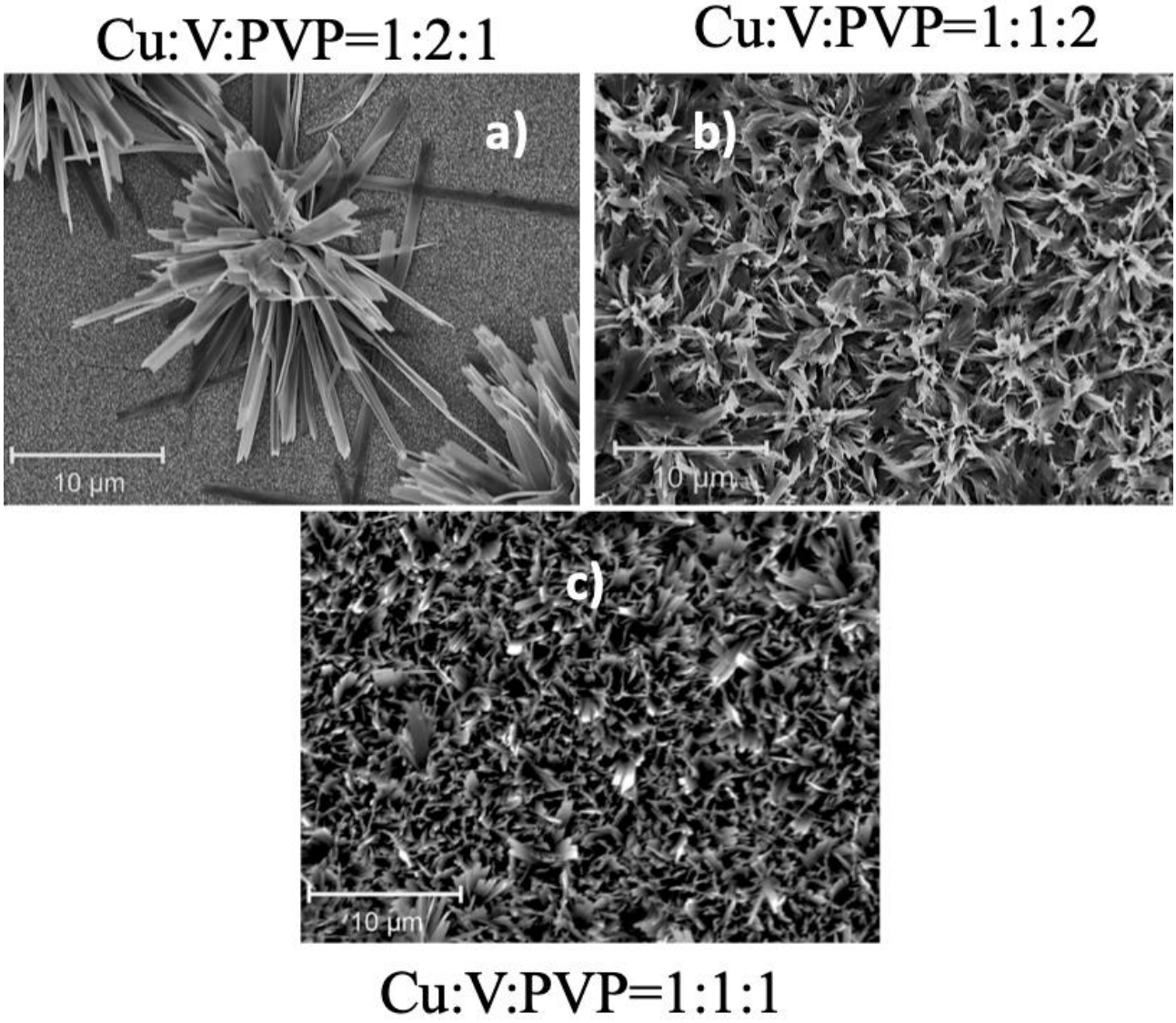

Figure S4. Representative SEM images of samples prepared with different ratios between copper, vanadium precursors and polyvinylpyrrolidone (PVP). (a) Image from a sample deposited using a Cu:V:PVP=1:2:1; (b) image from a sample deposited using a Cu:V:PVP=1:1:2 and (c) image from a sample deposited using a Cu:V:PVP=1:1:1.

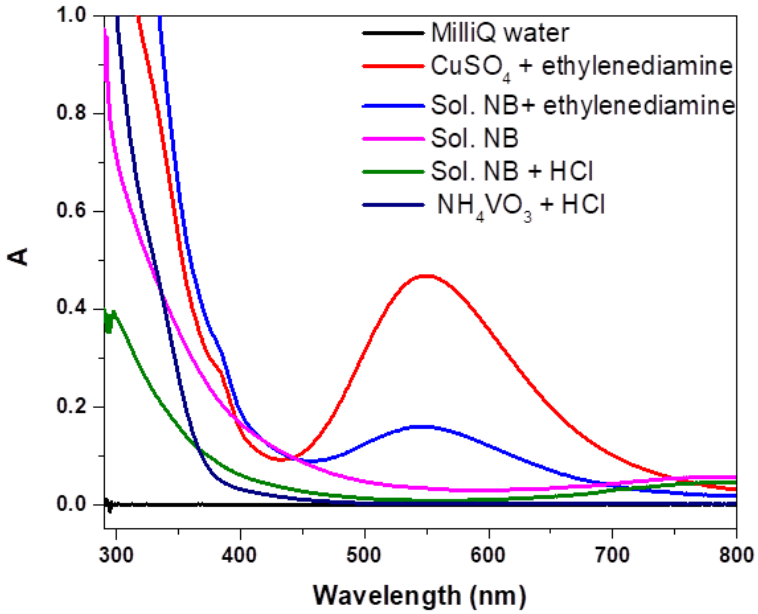

Figure S5. UV-Vis spectra of the working solution after the hydrothermal synthesis (Sol. NB). Upon ethylenediamine (en) introduction (red curve), the absorption band of the $[Cu(en)_2(H_2O)_2]^{2+}$complex centered at $\lambda \approx 550$ nm appears.

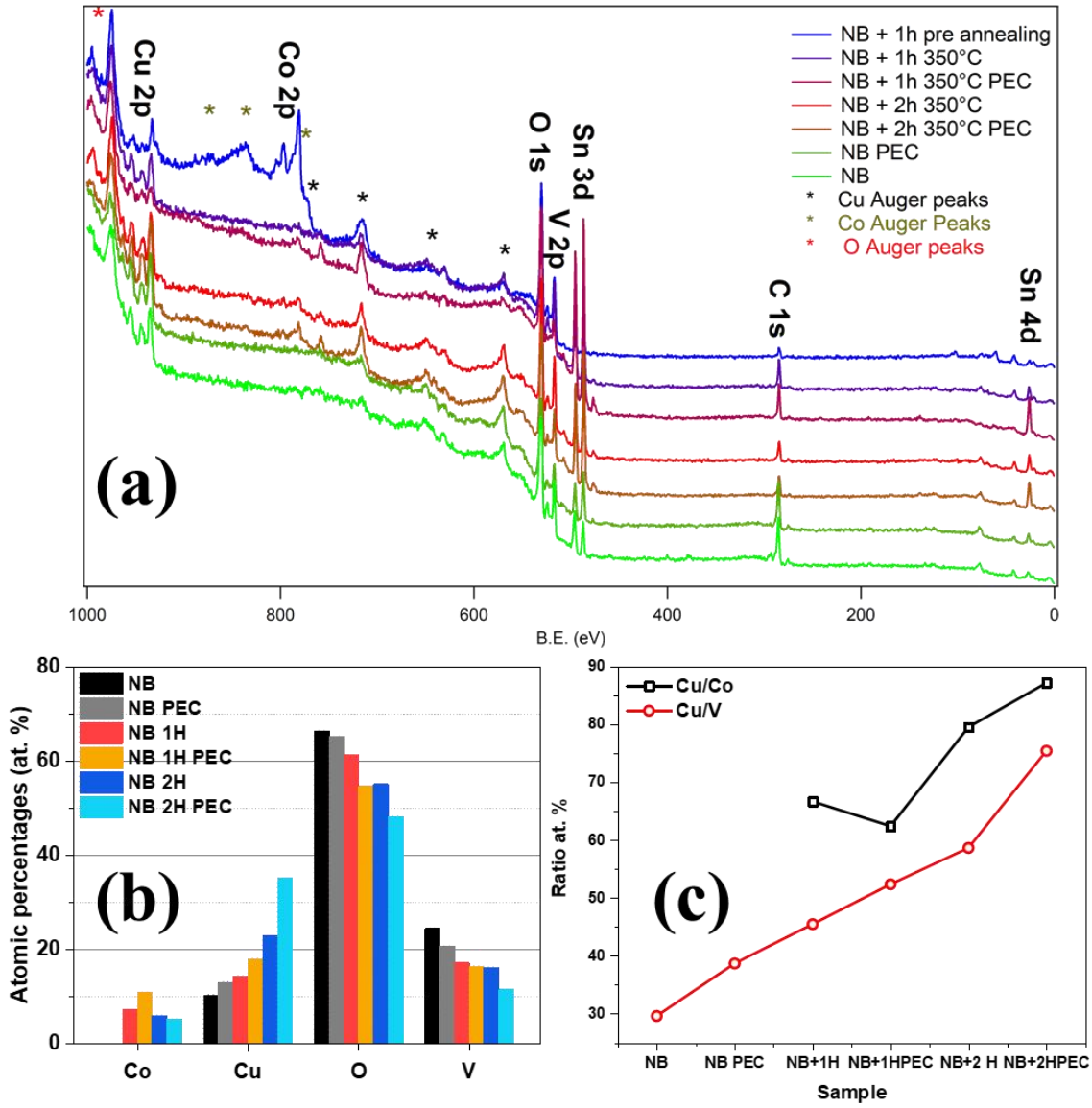

Figure S6. (a) X-ray Photoelectron Spectroscopy (XPS) survey scans before and after the PhotoElectroChemical (PEC) tests. (b) Bar plot of the corresponding atomic percentages (at.%). (c) Cu/Co and Cu/V at.% ratios for the different target specimens. The thickness of CoO_X overlayer was aproximately calculated by XPS data (Co 2p/Cu+V 2p) and found close to 0.8 equivalent nm [1].

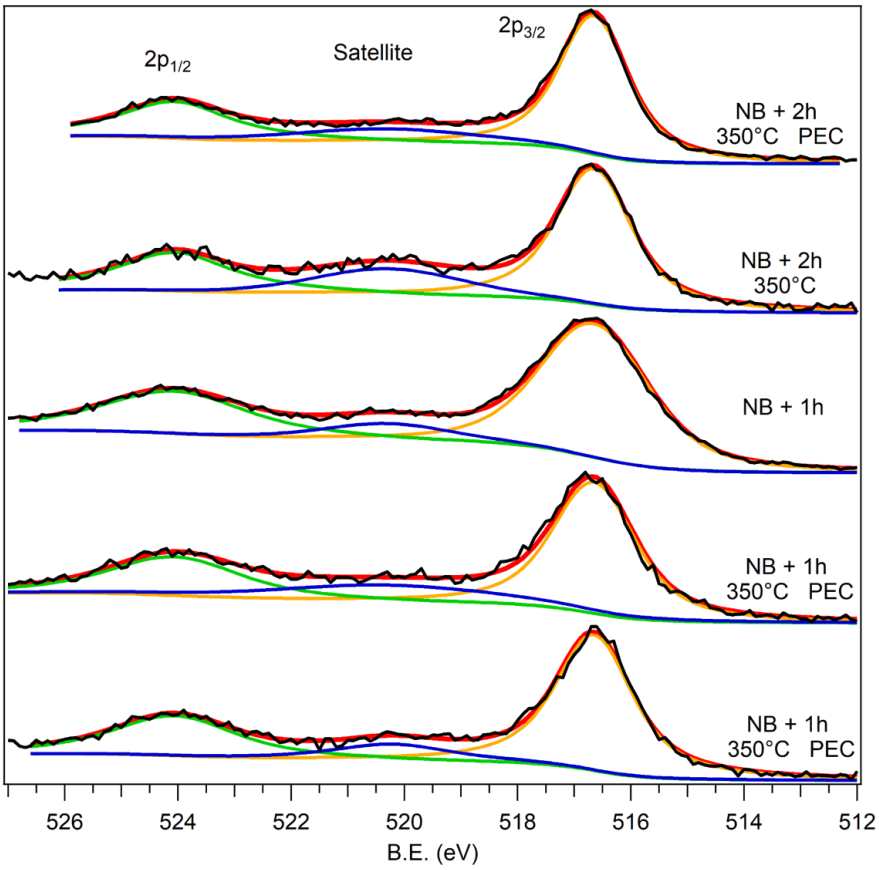

Figure S7. High resolution V 2p XPS spectra. In the figure are marked the position of the peaks $2p_{3/2}$ and $2p_{1/2}$ of vanadium and the satellite related to the oxygen contamination of the X-ray source.

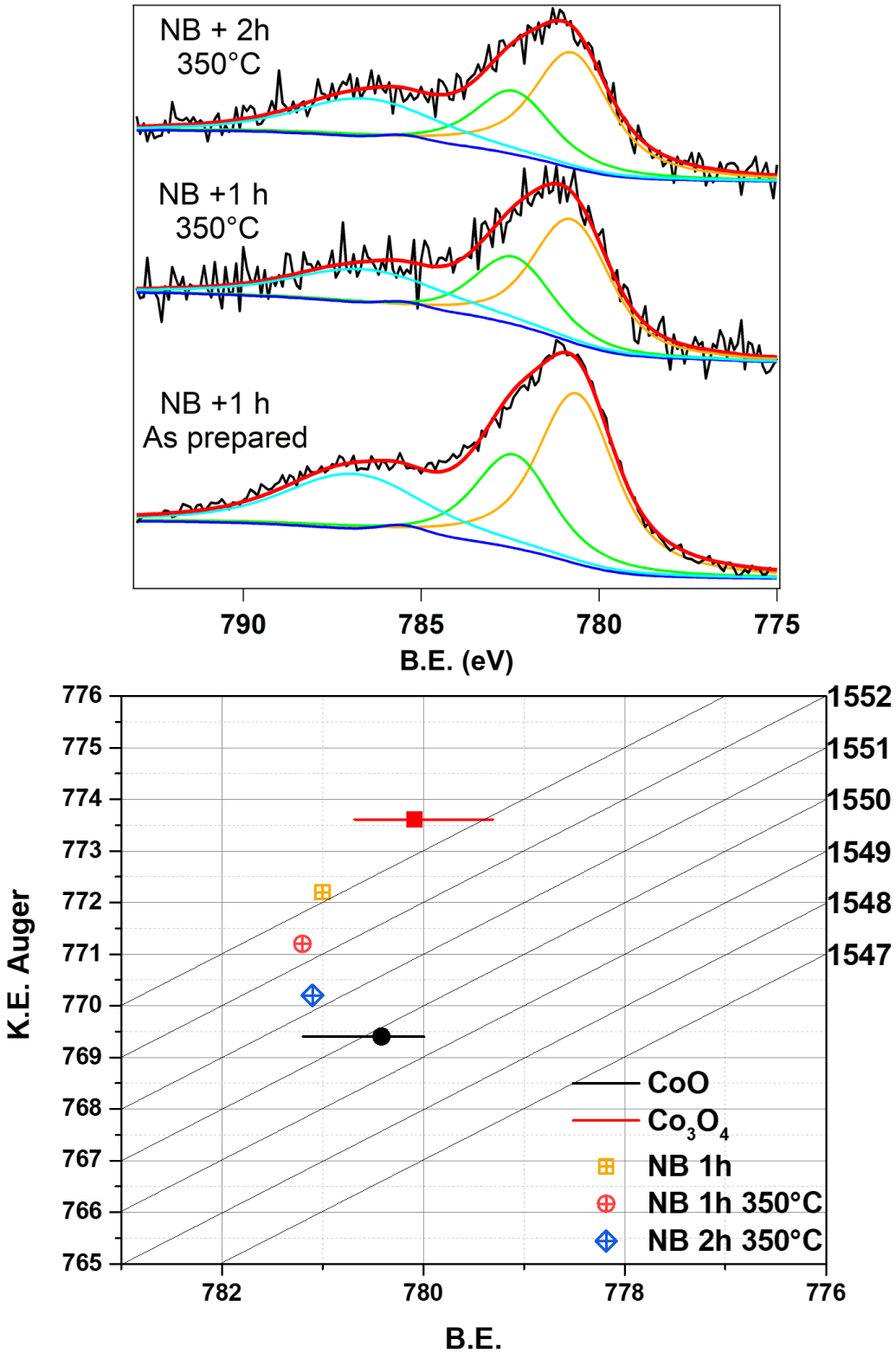

Figure S8. High resolution $Co2p_{3/2}$ XPS spectra and Wagner plot for Co α-parameter. As can be observed, the annealing process has only a modest influence on the peak shape.

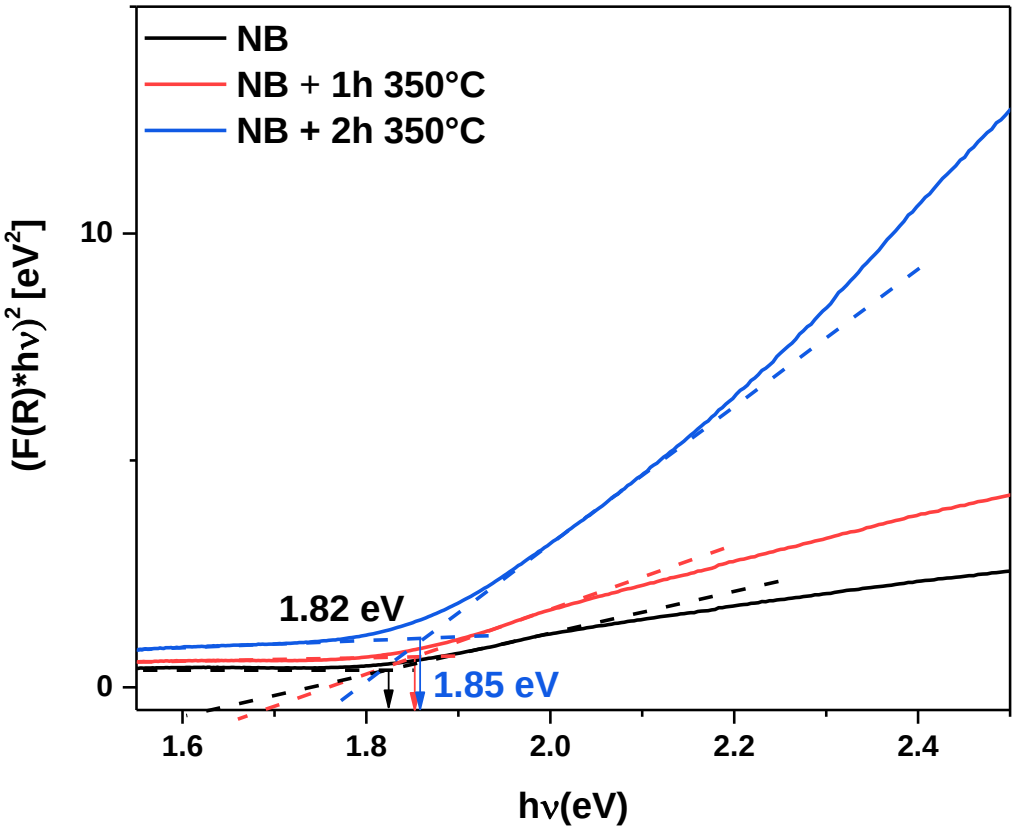

Figure S9. Tauc plots of the extrapolation of sample band gap values.[2]

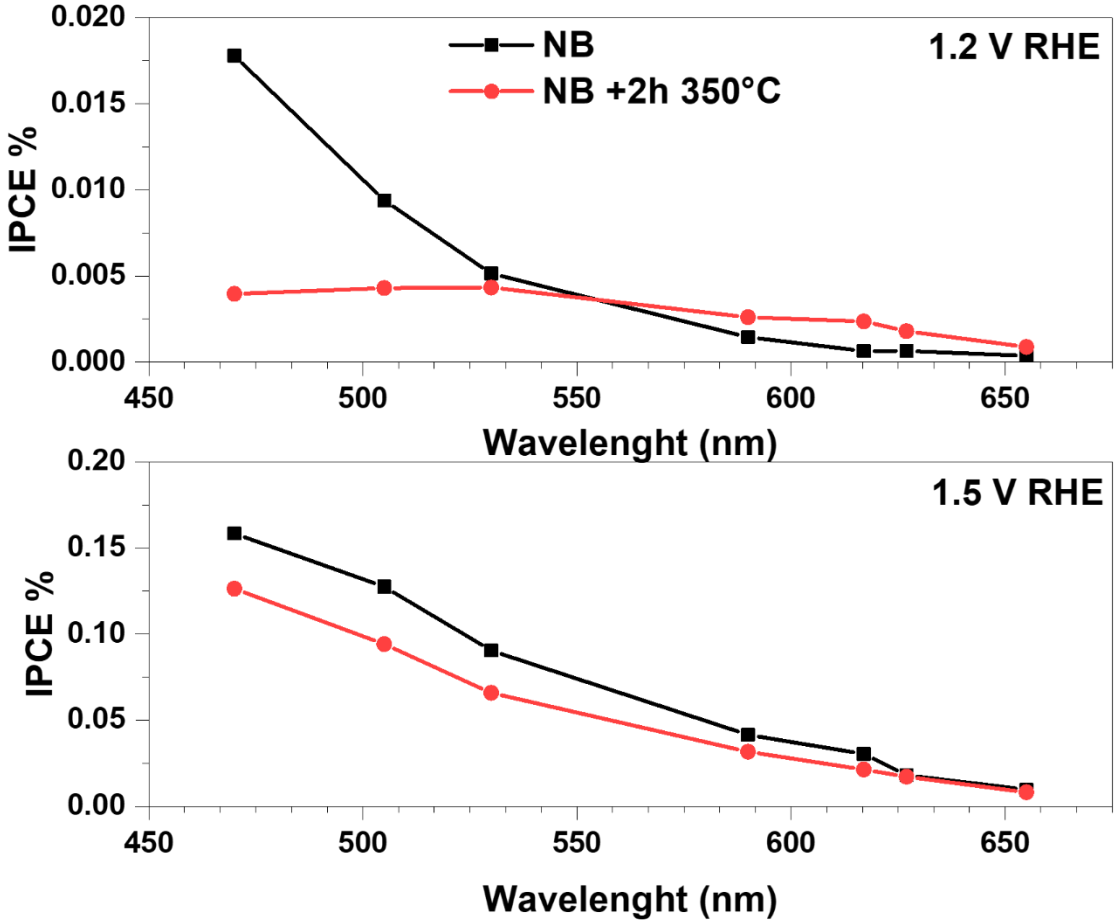

Figure S10. Incident Photon Conversion Efficiency (IPCE) plots acquired for samples NB and NB 2h 350°C.

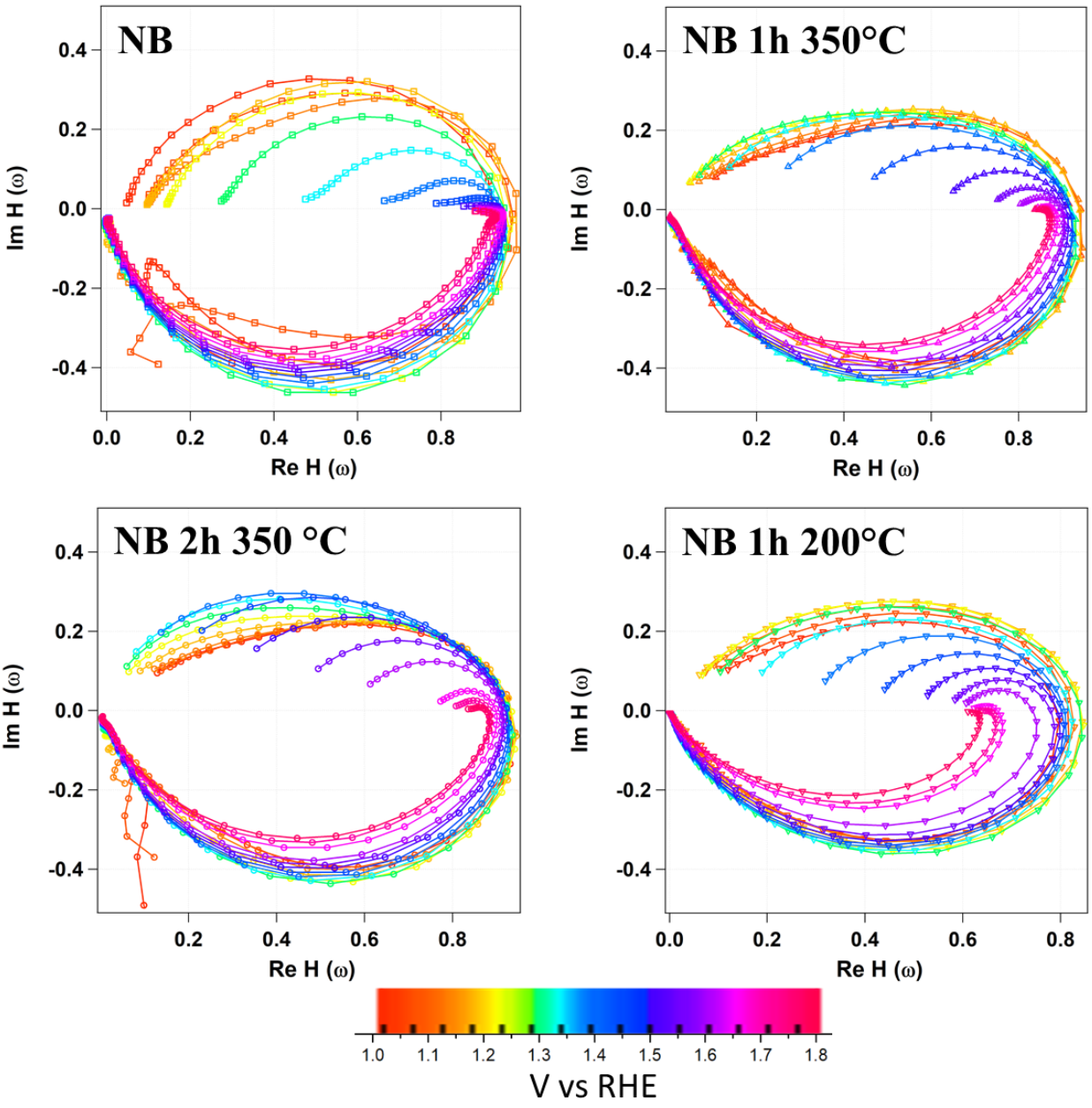

Figure S11. Intensity Modulated Photocurrent Spectroscopy (IMPS) Nyquist plots for the CuV_2O_6 NB sample, NB 1h, NB 2h and NB 1h 200. The reported data were normalized by multiplication by the factor $[C_H/(C_H+C_{SC})]^3$. This factor is close to 1 when $C_{SC} << C_H$. Csc is estimated from the time constant of the cell (the frequency corresponding to the minimum of the imaginary part of H (ω) $\tau_{cell}=R_{cell}C_{sc}$) and C_H is assumed around 20μF/cm^2 as for semiconductor with intermediate carrier density[4].

Gärtner Equation

The Gärtner equation describes the hole flux that reaches the surfaces of a *n*-type semiconductor under illumination.[3,5] The holes are generated both in the field-free and in the space charge zone. The first type of holes can migrate only through diffusion processes, whereas the second type migrates towards the surface due to the electric field present in the space charge region:

$$EQE = \frac{j_H}{qP_0} = 1 - \frac{e^{-\alpha W_{SC}}}{1 + \alpha L_D} \qquad (\mathbf{1})$$

$$-\ln(1 - EQE) = \alpha W_{SC} + \ln(1 + \alpha L_D) \qquad (\mathbf{2})$$

$$W_{SC} = \sqrt{\frac{2\epsilon_r \epsilon_0 (\boldsymbol{V} - \boldsymbol{V_{FB}})}{qN_D}} \qquad (\mathbf{3})$$

EQE is the external quantum efficiency, that gives an indication on the goodness of the conversion of the photon flux to hole current, considering the absorption characteristic of the material.

In this equation j_H indicates the photogenerated holes due to the photon flux P_0. The ratio between these quantities is defined as the external quantum efficiency (that is very similar to HFI value). In addition α iss the material absorption coefficient, L_D is the hole diffusion length, and W_{SC} denotes the width of the space charge region inside the material. This value depends on the applied potential (V) with respect to the flat band potential (V_{FB}), on the dielectric constant of the material and on the donor concentration (N_D). In IMPS measurements, the value of HFI is interpreted as an estimation of EQE[5].

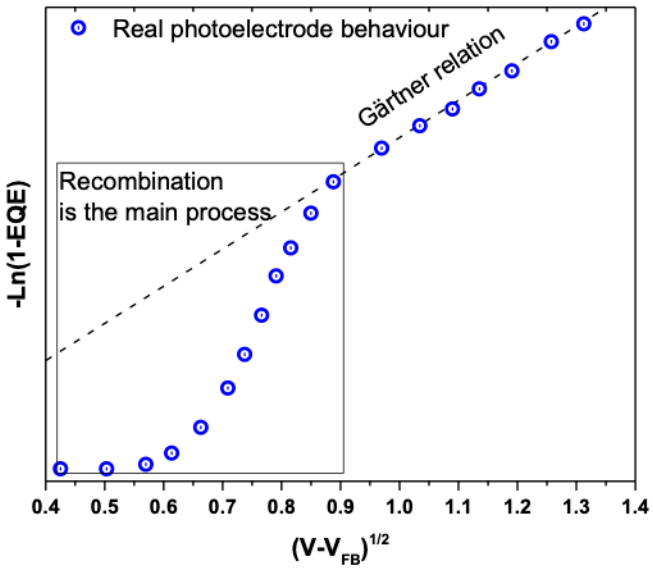

Figure S12. EQE dependence on the band bending of a real photoanode material (where loss mechanisms are also present), compared with the trend predicted by the Gärtner equation.

			1.2 V *vs.* RHE			1.5 V *vs.* RHE			
Vanadate phase	**V onset**	**J @ 1.5V (mA/cm^2)**	**k_{rec} (1/s)**	**k_{ct} (s^{-1})**	**η_{CT}**	**k_{rec} (s^{-1})**	**k_{ct} (s^{-1})**	**η_{CT}**	**Reference**
CuV_2O_6	1.2	0.2							[6]
$Cu_2V_2O_7$	1.1	0.12							[6]
$Cu_2V_2O_7$	1.1	0.06	7	30	81	0.5	30	98	[7]
$Cu_3V_2O_8$	1.0	0.12	15	50	77	2	60	97	[7]
$Cu_{11}V_6O_{26}$	1.0	0.1	30	45	60	7	70	91	[7]
$Cu_5V_2O_{10}$	1.3	0.025	200	5	2	80	28	26	[7]
NB (CuV_2O_6)	**1.2**	**0.09**	**11**	**2**	14	**0.01**	**0.06**	87	This work
NB+1h 350	1.4	0.03	2.7	0.07	3	0.15	0.12	44	This work
NB+2h 350	1.4	0.02	1.3	0.02	2	0.15	0.43	74	This work
NB+1h 200°C	1.3	0.04	0.9	0.04	4	0.28	0.37	57	This work

Table S1. Comparison of PEC performances of the present copper vanadate specimens with selected literature data.

References:

(1) Drera, G.; Salvinelli, G.; Ahlund, J.; Karlsson, P. G.; Wannberg, B.; Magnano, E.; Nappini, S.; Sangaletti, L. Transmission Function Calibration of an Angular Resolved Analyzer for X-Ray Photoemission Spectroscopy : Theory vs Experiment. *J. Electron Spectros. Relat. Phenomena* **2014**, *195*, 109–116

(2) Kwolek, P.; Szaciłowski, K. Photoelectrochemistry of N-Type Bismuth Oxyiodide. *Electrochim. Acta* **2013**, *104* (February), 448–453.

(3) Zachäus, C.; Abdi, F. F.; Peter, L. M.; Van De Krol, R. Photocurrent of BiVO4 Is Limited by Surface Recombination, Not Surface Catalysis. *Chem. Sci.* **2017**, *8* (5), 3712–3719.

(4) van de Krol, R. *Photoelectrochemical Hydrogen Production*; Van De Krol, R., Gärtzel, M., Eds.; Springer US, 2012.

(5) Peter, L. M. Dynamic Aspects of Semiconductor Photoelectrochemistry. *Chem. Rev.* **1990**, *90*, 753–769.

(6) Guo, W.; Chemelewski, W. D.; Mabayoje, O.; Xiao, P.; Zhang, Y.; Mullins, C. B. Synthesis and Characterization of CuV_2O_6 and $Cu_2V_2O_7$: Two Photoanode Candidates for Photoelectrochemical Water Oxidation. *J. Phys. Chem. C* **2015**, *119* (49), 27220–27227.

(7) Jiang, C. M.; Segev, G.; Hess, L. H.; Liu, G.; Zaborski, G.; Toma, F. M.; Cooper, J. K.; Sharp, I. D. Composition-Dependent Functionality of Copper Vanadate Photoanodes. *ACS Appl. Mater. Interfaces* **2018**, *10* (13), 10627–10633.